Proceedings of ASME Turbo Expo 2011
GT2011
June 6-10, 2011, Vancouver, British Columbia, Canada

GT2011-45254

DETAILED HEAT TRANSFER DISTRIBUTIONS IN ENGINE SIMILAR COOLING CHANNELS FOR A TURBINE ROTOR BLADE WITH DIFFERENT RIB ORIENTATIONS

Christopher LeBlanc and Srinath V. Ekkad[1]
Mechanical Engineering Department
Virginia Tech
Blacksburg, VA 24061

Tony Lambert and Veera Rajendran
Rolls-Royce Corporation
Indianapolis, IN 46214

ABSTRACT

Detailed Nusselt number distributions are presented for a gas turbine engine similar internal channel geometry used for cooling a modern first stage rotor blade. The cooling design has one leading edge channel and a three-pass channel that covers the rest of the blade. The simulated model, generated from the midspan section of an actual cooling circuit, was studied for wall heat transfer coefficient measurements using the transient liquid crystal technique. The model wall inner surfaces were sprayed with thermochromic liquid crystals, and a transient test was used to obtain the local heat transfer coefficients from the measured color change. Results are presented for a nominal channel inlet leading edge channel Reynolds number of 10700 and a channel inlet three-pass channel Reynolds number of 25500. Detailed heat transfer measurements are presented for the simulated leading edge, first pass, second pass and third pass interior walls for different rib configurations. The channels were studied for smooth, 90^o ribs, and angled ribs geometries in addition to ribs on the divider walls between adjacent passages. Overall pressure drop measurements were also obtained for each passage. Some of these results are compared with the predicted heat transfer from standard correlations used in design practices. Results show very complicated heat transfer behavior in these realistic channels compared to results obtained in simplistic geometry channels from published studies. In some cases, the Nusselt numbers predicted by correlations are 50-60% higher than obtained from the current experiments.

INTRODUCTION

Gas turbine engines are the work horse of modern day propulsion and ground based power generation systems. As demand for power has increased, turbine inlet temperatures have risen significantly resulting in need for more efficient cooling schemes for first stage turbine airfoils which face the brunt of the post combustion gases. In advanced gas turbine blades, the internals of the blades are cooled convectively by passing cooler air bled off from compressor through complex passages. These passages are typically cooled by impingement, ribs/turbulators, or pin fins to enhance heat transfer. Rib turbulated channels are the most commonly used cooling features for internals of turbine blades. Han [1] showed that the heat transfer inside turbine blade passages is influenced by channel aspect ratio, rib configuration, and the flow Reynolds number. The aim was to find optimal values for rib geometry such as rib height, pitch, and angle of attack (60^o, 90^o, etc.). Han [2] provided heat transfer results for square and rectangular turbulated channels with different rib spacings. This study provided a correlation for estimating heat transfer inside turbulated channels and is still used by gas turbine designers to estimate cooling requirements for turbine blades in modern engines. Han et al. [3] studied the heat transfer augmentation with a variety of rib configurations. They showed that complex rib formations can enhance heat transfer without imposing significant penalty on pressure drop. Zhang et al. [4] studied full and partial ribbed walls in triangular channels that represent the leading edge region channel for turbine airfoils. They developed and presented a correlation for predicting heat transfer for triangular channels with ribs. Taslim et al. [5] also studied leading edge channels but with more realistic curved surfaces. Ekkad and Han [6] used a transient liquid crystal technique to determine detailed heat transfer coefficients in a ribbed two–pass duct. They varied channel Reynolds numbers and rib geometries for a square duct. They clearly showed the local enhancement caused by flow separation and reattachment downstream of the ribs and the associated secondary flow induced heat transfer enhancement. Many of the above studies have focused on simplified channel geometries. Han et al. [7] provided an expansive literature survey in their book on various studies that have been performed on ribbed coolant channels. However, little data has been presented for all sides of the channel geometries in the literature which is the focus of the current study.

The designers use correlations developed using simplified geometries and apply them to the complex channel geometries of the actual blade. However, there has been little or no data available to evaluate the validity of the predicted values for the complex channels. Engine tests tend to obfuscate the effects of internal cooling since they are altered by external heat transfer (film cooling, etc.). Poser et al. [8] conducted transient heat transfer experiments in a model of a multi-pass gas turbine blade cooling circuit. The inner surface of the

[1] ASME Fellow; Corresponding Author; sekkad@vt.edu

plexiglass model was coated with thermochromic liquid crystals in order to determine the internal heat transfer coefficients. The experiments were conducted with an engine-representative Reynolds number, Mach number and heat flux direction as in a real blade. They evaluated their method and performed an uncertainty analysis which demonstrated robustness for the investigated geometries. This study is the first to focus on an actual engine type internal cooling configuration and make detailed heat transfer measurements in such channels and compare to standard correlation predictions used by designers.

In the current study, engine similar coolant channel geometries with ribs are studied. The leading edge channel also simulated bleed for showerhead film cooling and tip cooling through the blade tip dust holes. The leading edge channel and the three pass channels are simplified to remove curved surfaces as seen in real designs. This is to enable better viewing with the camera. All the experiments are run at the engine Reynolds numbers based on channel entrance conditions. The heat transfer enhancement results are compared for different rib configurations. The leading edge channel and the three pass channel had separate coolant entry channels. Pressure drop results are also presented.

EXPERIMENTAL METHODOLOGY

Figure 1 shows the experimental setup used for the study. Compressed and metered air enters from a 50-mm round pipe and expands to a 35.56 x 15.24 cm^2 plenum. The plenum allows the flow for a uniform velocity before passing through the mesh heater. The length of the plenum is 52-cm before the heater. At the exit of the plenum, a mesh heater constructed of 304-stainless steel woven wire with a wire diameter of 20 microns is placed. The mesh heater used is similar to the heaters presented by Esposito et al. [9]. A 2-cm spacer separates the mesh heater and the reduction nozzle leading to the test section to complete the test rig. Power is supplied to the mesh heater by a welding machine power source providing low voltage, high amperage DC power. The test section walls are constructed from clear, acrylic, low thermal conductivity material to reduce conduction losses during the experiment and to allow for visibility of liquid crystal color changes.

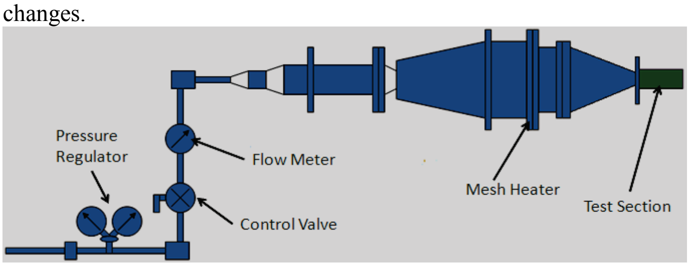

Figure 1 Experimental Set up

The test section material is 0.64 cm thick clear acrylic which is a low conductivity, low thermal diffusivity material that is necessary for the transient liquid crystal technique. A thin layer of thermochromic liquid crystal paint (SPN R25C5W) was applied on the inside wall of test surface. The liquid crystal paint has a color play range between 25°C and 30°C. A thin layer of black paint is applied behind the liquid crystal paint to provide a background for the color changes during the experiments. The liquid crystal paint was calibrated "in situ" during the test using a foil thermocouple glued to the target surface. Since the color is calibrated in-situ during each experiment, the issue of lighting, camera placement, and other conditions do not affect the calibration curve. A new calibration curve is generated for each specific test. The color is expressed in Hue and calibrated to the corresponding thermocouple temperature. A Canon FS2000 color CCD camera capable of capturing images at a frame rate of 30 frames per second and resolution of 1024x768 pixels is used to record the transient response of the liquid crystal color change. The camera stores data locally on an SDHC card and transfers to a PC later through a USB connection.

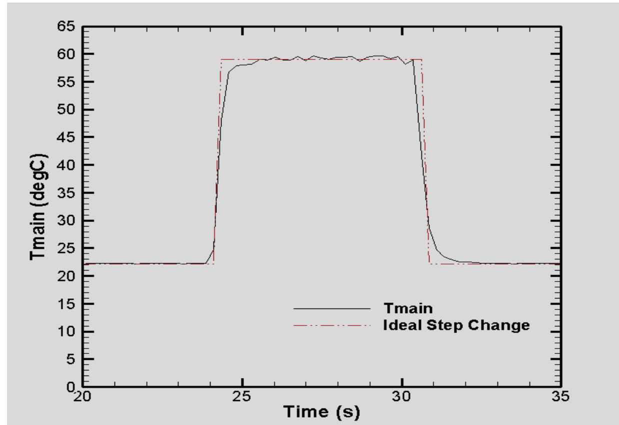

Figure 2 Step Change in Mainstream Temperature obtained from Mesh Heater Response

The mesh heater allows the assumption of a true step change in mainstream temperature during the transient test. The heater reaches steady state temperature in less than 33 milliseconds and therefore a step change in temperature is assumed in the calculations. The heater temperature was measured using an IR camera with a 60 Hz frame rate. After capturing the images, the IR camera images showed that the temperature on the heater was uniform immediately at the first image which is 33 milliseconds after initiation of the heater and remained steady after that. Figure 2 shows the temperature response of the mesh heater during an experiment. A true step change is also shown on the figure. However, the thermocouple has a time constant of 1 second which is larger than the IR camera response and therefore cannot show the instantaneous temperature change. The thermocouple response shows much higher time to capture the heater response due to higher time constant.

During the experiment, the flowrate corresponding to the test Reynolds number is set using the orifice meter. Adequate time is given for the test section to reach steady state temperature with the mainstream flow prior to switching on the heater. The camera starts recording frames at the same time as the heater is switched on and the test starts. Thermocouples on the target surface (placed in the corner region of the view area of the camera) and in the flow upstream of the test section, record wall and mainstream temperatures respectively. There are additional thermocouples in the turn region of every passage to monitor the change in mainstream temperature from inlet to exit during the experiment. This change was a small drop of 2^{o}C during the experiment form inlet to exit temperature for each pass. We, however, used the average temperature from passage entrance to passage exit for each passage for data reduction.

The transient method used in the experiment is based on the transient heating of a semi-infinite solid. A 1-D transient conduction model is used to analyze the surface temperature response [10]. Due to the low thermal conductivity of the acrylic target plate and short test duration of 10 seconds, lateral conduction can be ignored and the test plate can be treated as a semi-infinite medium into the plate. Imposing a convective boundary condition on a semi-infinite solid allows the solution of the surface wall temperature history for a given heat transfer coefficient. The transient response of the surface temperature is given by Eq (1).

$$\frac{T_w - T_i}{T_m - T_i} = 1 - \exp\left(\frac{h^2 \alpha t}{k^2}\right) erfc\left(\frac{h\sqrt{\alpha t}}{k}\right) \quad (1)$$

Where T_w is the wall temperature, T_i is the initial temperature of the test section, T_m is the mainstream temperature before the flow enters the test section, h is the local heat transfer coefficient, α is the thermal diffusivity of acrylic, k is the thermal conductivity of acrylic, and t is time. To be more accurate, the flow temperature (T_m) was always the average of inlet and outlet temperature for each passage during that particular run. Although only one wall temperature and time data pair is needed to solve the equation for the heat transfer coefficient, to reduce errors, data is collected over the range of the liquid crystal color play and test duration. Since the liquid crystal paint chosen was able to give wall temperatures over a wide range of temperatures, a regression technique was used to eliminate random errors in recorded local wall temperatures which range up to 30 seconds of data taken at 30-frames/second. The regression technique puts all terms of Eq. (1) to the one side of the equation and solved for all points of temperature data for each pixel. This resulted in a residual error for each time-temperature data pair. The residual error was minimized using a least squares solution for the heat transfer coefficient that best fit all data. This also reduced the random camera read errors (due to lighting variations) of the liquid crystal paint and also relaxes the dependence on the initial temperature of the target plate on the results. The heat transfer coefficient was then converted into the dimensionless form. The Nusselt number, Nu_d is given in Eq (2).

$$Nu_d = \frac{hd_h}{k_{air}} \quad (2)$$

A simple algorithm that allowed for the systematic varying of experimental parameters in recorded data was used to estimate the overall uncertainty of the results for both parts of the study. This was calculated for an average heat transfer coefficient value for the experiments. Using the single temperature method resulted in the uncertainty in h at about ±12%. However, when the regression analysis technique was applied, the overall uncertainty dropped to ±7%. Since this is a 2-D plate with uniform thickness, the variation in uncertainty is dependent on maximum to minimum heat transfer coefficient and hence the penetration depth. Due to the shortness of experimental duration, the variation was from ±5-8.5%. The uncertainty in flow Reynolds number based on orifice flow meter measurement was assessed to be ±3%. The method of Kline and McKlintock [11] was used to assess the overall uncertainty in heat transfer coefficient and flow Reynolds number measurement.

TEST SECTION

The test geometry for this study was derived from the mid-span section of an actual cooled turbine first stage rotor blade. Figure 3a shows the cross-section of the blade. The given channel geometry includes one leading edge channel with its own coolant feed from the base of the channel and a three pass channel where the flow enters the channel adjacent to the leading edge channel and passes through two 180° turns before being ejected through a row of holes at the trailing edge. The leading edge channel coolant is ejected through two rows of showerhead film holes at the leading edge of the airfoil. Figure 3b shows the simplified geometry obtained by adding sharp corners to the channels to provide ease for fabrication and testing. The leading edge and trailing edge channels were approximated by triangular channels. A rectangular channel approximates the first pass channel of the triple pass and a trapezoidal channel approximates the second pass. The channel dimensions are shown in Table 1. The hydraulic diameters are also shown for each channel. The inlet channel Reynolds number is fixed to the specified design condition. The channel length is extruded for the same channel size simulating a 2-dimensional channel with a length of 12 cm.

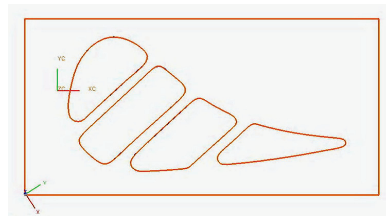

Figure 3a Actual channel geometry

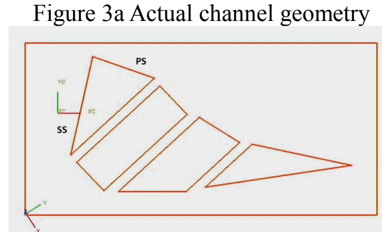

Figure 3b Simplified channel geometry

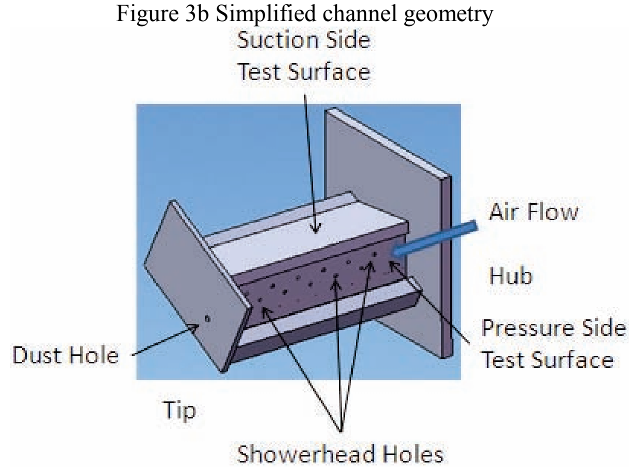

Figure 4a Leading edge channel geometry

Figure 4a shows the leading edge channel geometry with indicated flow paths and also the leading edge rows of holes and one dust hole. The flow enters at the hub of the channel and ejects out through the film holes and dust hole at the tip. Figure 4b shows the two views of the triple pass channel geometry. The top figure shows the pressure side view and the bottom figure shows the suction side view of the three pass channel. The flow enters the first pass at the hub and flow towards the tip. Some coolant is ejected through a dust hole at the tip. The flow then turns 180° into the second pass and travel from tip to hub and then turns 180° into the third pass flowing from hub to tip. Most of the coolant is ejected through a row of holes on the trailing edge and some coolant is ejected through two dust holes at the tip. Dust holes are typically provided to clean out the dust that might collect at 180° bends. Usually, a small amount of flow is ejected out of the dust hole.

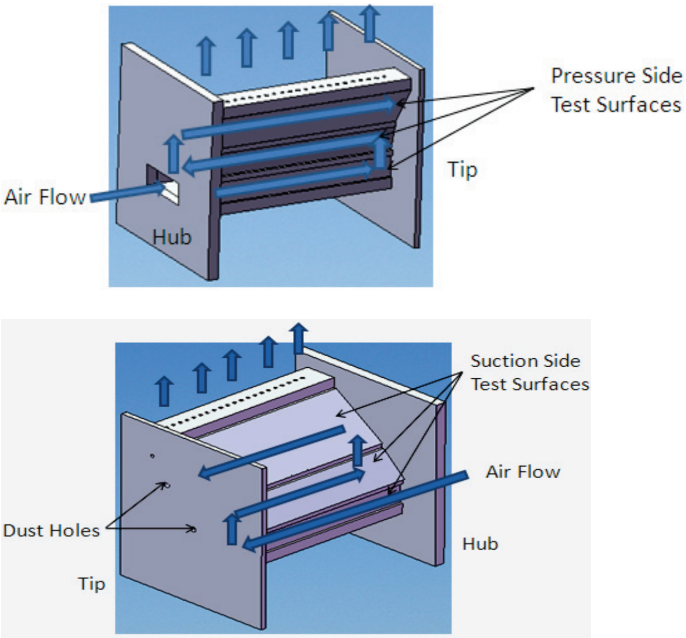

Figure 4b Triple pass channel geometry

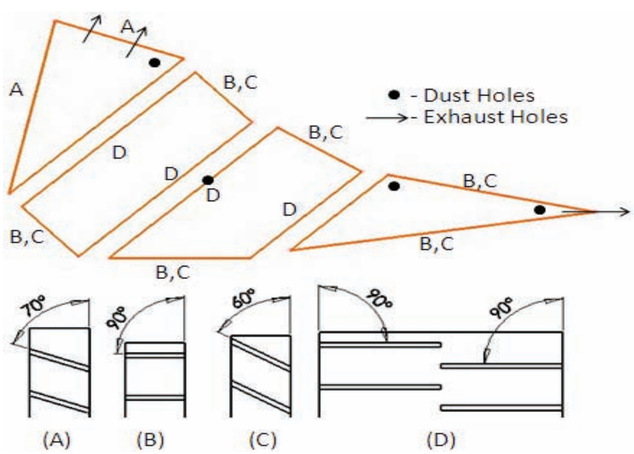

Figure 5 Rib arrangements studied

Figure 5 shows the rib configurations for each wall. For the leading channel, the rib configuration was rib angles at 70^o to the incoming flow and is shown in (A) configuration. The rib pitch and height are given in Table 1. For the triple pass, two rib configurations (B) and (C) are studied for the pressure side and suction side surfaces. The configuration (D) with the split 90^o ribs is only for the divider walls. For the leading edge channel, only smooth and one ribbed configuration (A) are studied. For the triple pass channel, smooth, Configuration (B) and (D) together, Configuration (C) by itself, and Configuration (C) and (D) together are studied. All these configurations are listed in Table 1. The divider wall thickness is 3.18 mm. The heated flow is on both sides of the divider walls ensuring no heat loss through the divider walls.

Table 1 presents all the test cases that were run on the overall test geometry. Details on the various rib configurations including angle, rib pitch to height ratio (P/e) and the rib height to channel hydraulic diameter ratio (e/D_h). The channel dimensions are also presented for each of the four channels. The rib pitch to height is similar for all channels at 8.8. The rib height to channel hydraulic diameter is 0.082 for the leading edge channel and 0.066 for the triple pass channel. Also, it is important to note that the ribs used in the current study are rounded edges similar to engine geometry whereas the correlations for designers were developed from measurements on square edged ribs.

Table 1 Test Cases, Channel and Rib geometries

Case	Channel	Geometry	Rib configuration	P/e	e/Dh	Channel dimensions (mm)
Case 1	LE channel	Triangular	Smooth	0	0	3.5289, 3.163, 2.016
Case 2	LE channel	Triangular	(A)	8.8	0.082	3.5289, 3.163, 2.016
Case 3	First Pass	Rectangular	Smooth	0	0	3.502, 1.203, 3.502, 1.203
Case 4	First Pass	Rectangular	(B) & (D)	8.8	0.066	3.502, 1.203, 3.502, 1.203
Case 5	First Pass	Rectangular	(C) & (D)	8.8	0.066	3.502, 1.203, 3.502, 1.203
Case 6	First Pass	Rectangular	(C)	8.8	0.066	3.502, 1.203, 3.502, 1.203
Case 7	Second pass	Triangular	Smooth	0	0	1.469, 3.404, 2.081, 2.25
Case 8	Second pass	Trapezoidal	(B) & (D)	8.8	0.066	1.469, 3.404, 2.081, 2.25
Case 9	Second pass	Trapezoidal	(C) & (D)	8.8	0.066	1.469, 3.404, 2.081, 2.25
Case 10	Second pass	Trapezoidal	(C)	8.8	0.066	1.469, 3.404, 2.081, 2.25
Case 11	Third Pass	Triangular	Smooth	0	0	3.125, 1.971, 4.545
Case 12	Third Pass	Triangular	(B) & (D)	8.8	0.066	3.125, 1.971, 4.545
Case 13	Third Pass	Triangular	(C) & (D)	8.8	0.066	3.125, 1.971, 4.545
Case 14	Third Pass	Triangular	(C)	8.8	0.066	3.125, 1.971, 4.545

RESULTS AND DISCUSSION

Detailed heat transfer distributions were measured for a nominal channel entrance Reynolds number of 11,000 for the leading edge channel and a channel entrance Reynolds number of 25,500 for the triple pass with different rib channel configurations. Leading channel experiments were run independently as the leading edge channel and the triple pass do not share the same entrance plenum.

Figure 6 presents detailed heat transfer (Nusselt number) distributions for different surfaces of the internal cooling channels for a leading channel with Configuration A ribs and a triple pass channel with Configuration (C) ribs and Configuration (D) ribs on the divider walls. The divider walls were not considered for the heat transfer measurement due to logistical difficulties. The arrows next to each contour plot show the direction of the flow with hub and tip markings for each end of the channel length. The leading edge triangular channel shows much higher heat transfer coefficients on the pressure side of the channel where the coolant ejection holes compared to the suction side surface. This is expected as the coolant will migrate towards the film holes thus reducing the coolant near the suction side wall. The hole locations are clearly seen with small circles in the channel middle. Also, the heat transfer is higher around the holes due to acceleration of the coolant towards the ejection hole. This has been observed by Ekkad et al. [12] in their study of ejection holes in between ribbed surfaces.

From the triple pass results, we can see that the secondary flows are clearly induced by the rib angles on all surfaces. The inlet flow into the first pass clearly produces significantly higher Nusselt numbers due to inlet effects. As the flow moves upward from the hub to the tip of first pass, Nusselt numbers decrease along the surface. Near the tip, the flow turns 180^0 from a rectangular channel into a trapezoidal channel. Again, Nusselt numbers are significantly higher as the flow negotiates the turn and expands into the second pass. The Nusselt numbers decreases as the flow moves from tip to hub for this pass. Interestingly, pressure side Nusselt numbers do not significantly decreases as seen for the suction side. In the third pass, the flow turns 180^o into a narrow triangular channel with hole exits at one of the vertices (which is the trailing edge). The coolant negotiates the turn and immediately moves towards the trailing edge ejection holes resulting in high Nusselt numbers along the hub region of the pass and almost very little heat transfer enhancement at the tip region due to depleted coolant mass.

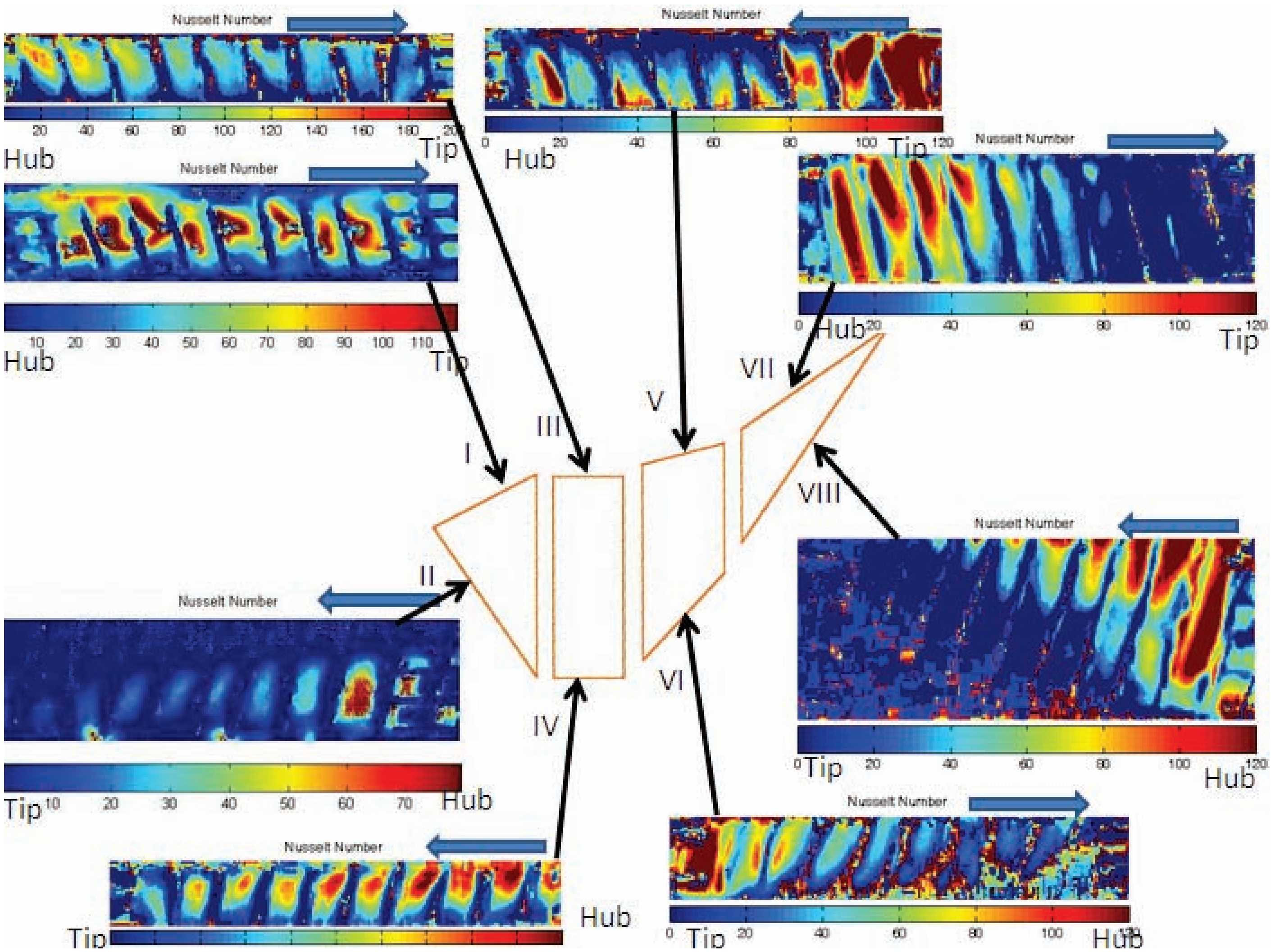

Figure 6 Detailed heat transfer (Nu) distributions for all channels with Configuration (C)

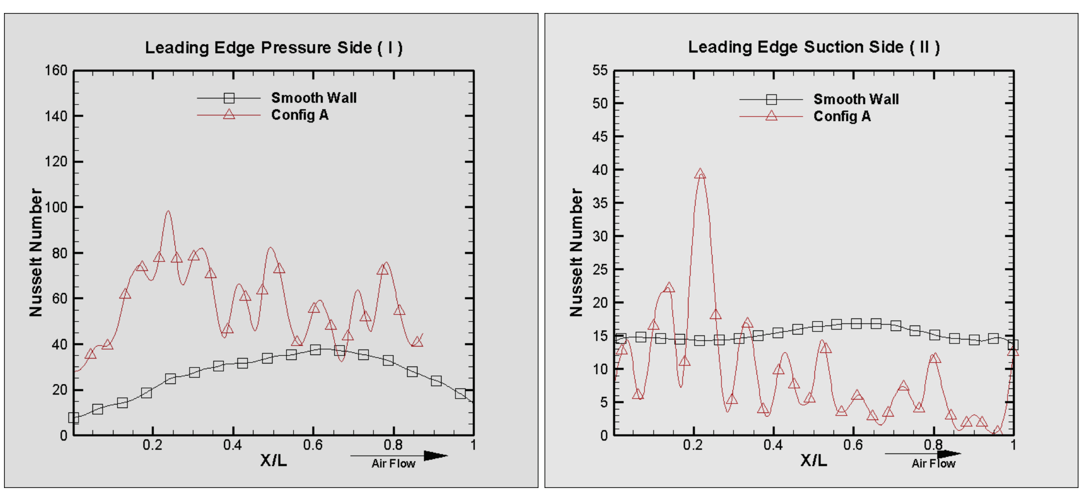

Figure 7 Spanwise averaged Nusselt number for the leading edge channel

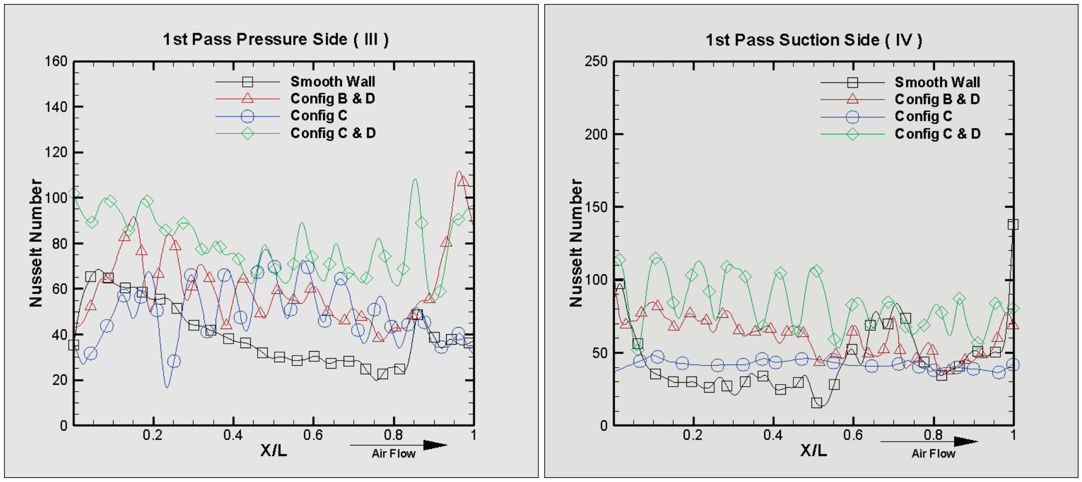

Figure 8 Spanwise averaged Nusselt number distributions for the First pass of the triple pass channel

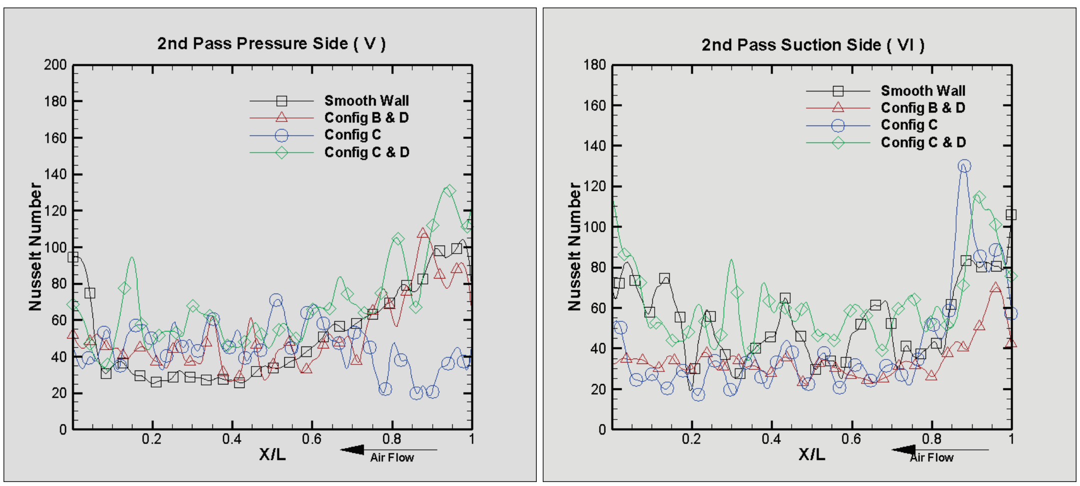

Figure 9 Spanwise averaged Nusselt number distributions for the Second pass of the triple pass channel

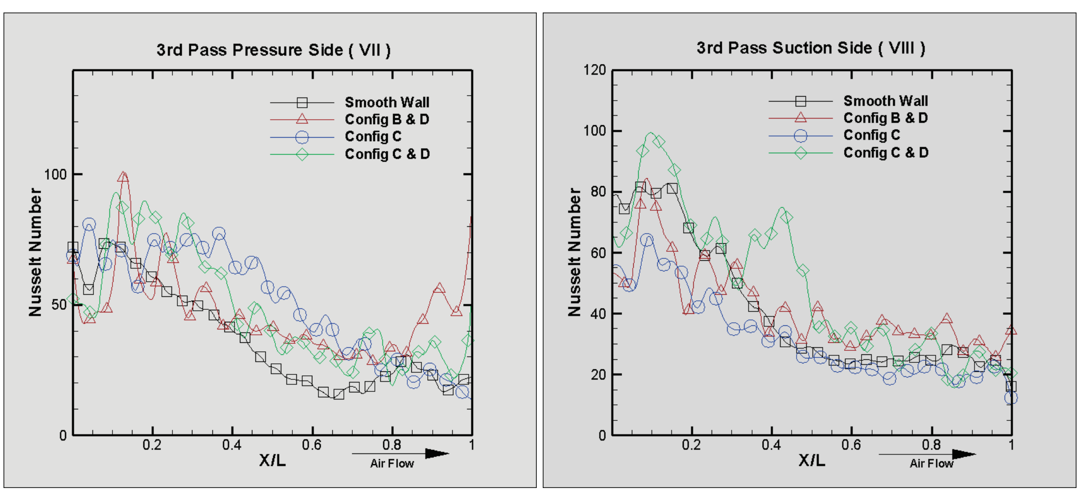

Figure 10 Spanwise averaged Nusselt number distributions for the Third pass of the triple pass channel

Spanwise averaged Nusselt numbers

Figure 7 presents the spanwise averaged Nusselt numbers for the leading edge channel for both pressure and suction surfaces. The Nusselt numbers are compared for a smooth channel versus a ribbed channel with Configuration (A) (Case 1 Vs. Case 2). The top figure shows the pressure side Nusselt numbers and the bottom figure shows the suction side Nusselt numbers as the flow enters from the hub. The axial distance is normalized by channel length. The pressure side surface shows significant enhancement over the smooth surface with almost 4 times enhancement at the entrance and about 1.5 times in the middle of the channel. It is to be noted that the flow is exiting through the holes on the leading edge and thus reducing the local Reynolds numbers in the channel. The coolant flow distribution for the smooth and ribbed walls may also be different along the passage as the presence of ribs can cause significant change in flow structure along the wall. On the suction surface, there is a degradation in heat transfer for the ribbed channel compared to the smooth channel. There is some enhancement in the near entrance region due to entrance effects and rib blockage. Once the flow enters the channel, the coolant migrates towards the pressure side wall as the film holes are along the pressure surface. This results in significant reduction in coolant flow along the suction surface. It is difficult to comprehend why the suction surface ribbed surface shows lower Nusselt numbers than the smooth surface. The only possible explanation for this is that more coolant migration occurs in the ribbed channel than for the smooth surface.

The detailed results clearly show the complex behavior of the coolant flow and the associated heat transfer distributions. The simplified channels geometries that are used in correlations cannot accurately predict the local behavior of the coolant and the Nusselt number distributions. However, the correlations can provide an overall average value which may be similar to averaged results from local measured heat transfer as seen in this study. However, the local cooling effectiveness may help determine failure locations and indicate lack of cooling in certain regions and may need to be addressed in design modifications.

Figure 8 presents the spanwise averaged Nusselt numbers for the first pass of the triple pass channel. Both pressure side and suction side surface Nusselt numbers are compared for cases 3-6 at channel inlet Reynolds number of 25,500. The pressure side surface with the angled rib and ribs on the divider wall (Conf. C) show the highest Nusselt number over the entire length of the channel. As expected, the smooth channel shows higher heat transfer at the entrance and decreases with increasing length and increases as the flow approaches the turn region at the end of the pass. The suction side surface also shows that Configuration (C+D) is the highest with Configuration (B+D) being slightly lower. Interestingly, when the ribs are not placed on the divider wall as in Configuration (C) only, the suction surface shows very low Nusselt numbers. The suction smooth surface behaves similar to the pressure smooth surface but has lower overall Nusselt numbers.

Figure 9 presents the spanwise averaged Nusselt numbers for the second pass of the triple pass channel comparing cases 7-10. In this case, the flow direction is reversed with entrance at X/L=1. Significant enhancement is seen immediately after the 180^{o} turn into the second pass. For the pressure side, all the four cases show similar levels of Nusselt number with the surface with angled ribs but no ribs on divider walls showing slightly lower values at the entrance region. Figure 10 also shows that the suction side heat transfer is significantly higher for the angled ribs with ribbed divider walls as in the case of the first pass pressure side. This may be because the flow is radially inward in this passage and may reflect similar behavior as the radially outward pressure side. The Configuration (B+D) ribbed channel shows lower Nusselt numbers than the other rib configurations.

Figure 10 presents the spanwise averaged Nusselt numbers for the third pass or trailing edge channel for cases 11-14. This is basically a very high aspect ratio triangular channel with exits at one of the corners which is the trailing edge of the blade. For the pressure side, the rib configuration (C) shows slightly higher Nusselt numbers in the middle of the channel. The Nusselt numbers are all high at the entrance of the pass right after the 180^{o} turn and then decreasing as the flow laterally leaves the channel. The smooth channel shows the lowest Nusselt numbers. For the suction surface, all the four geometries show similar levels with the smooth wall being slightly higher than the Configuration (C) only. In this case, the ribs direct the flow from the hub towards the trailing edge ejection holes causing lower heat transfer regions near the tip of the channel. Figure 7 shows the 2-D distributions for this geometry.

Comparisons with Correlations

Nusselt numbers and pressure drop were computed using correlations provided by Han and Park [2] for rectangular ribbed channels. The smooth channel Nusselt number was computed using the Dittus-Boelter correlation for smooth round pipe. Table 2 provides the comparison for first pass of the triple pass channel as it is rectangular. There is no correlation available for a trapezoidal channel or a triangular channel. Results are only compared for the first pass rectangular channel. Since the correlations use fully developed flow conditions, the experiment does not produce ideal conditions. Directly applying the correlation to the experimental rib configuration and channel geometry produces much higher predicted Nusselt numbers for the channel. There is a 50-60% lower measured Nusselt number than the predicted value. There are many reasons:

(a) Flow is not fully developed in the experiment because entrance length is small
(b) Ribs are rounded compared to sharp edged in the correlation causing lower enahncement
(c) Flow is not expanded uniformly due to sudden expansion to simulate engine type entrance conditions
(d) Exit conditions are different as the flow turns into the second pass in the experiment

Table 2 Comparison of Nusselt numbers from experimental data to correlation predictions

	Smooth	90-deg ribs	60-deg ribs
First Pass (Experiment)	42.5	60.64	82
First Pass (Correlations)	69	92	125
Difference (Corr/Exp)	1.62	1.52	1.52

Pressure Drop Results

The test section was instrumented with static pressure taps at the entrance of first pass, in the turn region between first pass and second pass and the turn region between the second pass and third pass. Pressure was also measured at the inlet of the leading edge channel. Results show the total pressure is lowest for the smooth channel with 90-deg ribbed channel showing the highest overall pressure drop. Table 3 provides the overall area averaged Nusselt numbers for each surface of the triple pass and the static pressure at the three measuring stations. Results show that the overall averaged heat transfer is lowest for the smooth surface and so is the overall pressure required to drive the flow through the smooth channels. Majority of the pressure drop occurs across the third pass for all the geometries with a value of around 4.5 kPa. Results show the heat transfer enhancement for the channels with angled ribs and divider wall ribs is significant with only a minor rise in overall pressure drop.

Table 3 Overall Nusselt numbers and gage pressure across the triple pass channel

Measured Average Nusselt Number				
Configuration	Smooth Wall	B+D	C	C+D
1st Pass Pressure Side	41.15	60.64	50.52	79.7
1st Pass Suction Side	44.21	60.65	42.47	83.37
2nd Pass Pressure Side	51.45	53.25	56.2	68.54
2nd Pass Suction Side	58.79	34.24	40.4	61.88
3rd Pass Pressure Side	37.16	46.94	40	48.84
3rd Pass Suction Side	41.69	52.09	35	48.96
Pressure Data (kPa)				
Configuration	Smooth Wall	B+D	C	C+D
1st Pass Entrance	4.995	5.3425	5.1	5.205
1st Turn Region	4.8575	5.0125	4.93	5.0425
2nd Turn Region	4.46	4.5075	4.48	4.5

CONCLUSIONS

Detailed heat transfer distributions are presented for a realistic turbine blade cooling circuit at engine representative Reynolds numbers. Different rib configurations have been studied to determine the effect on heat transfer and pressure drop. The results show 50-100% enhancement in heat transfer compared to smooth surface. The detailed distributions clearly show the effect of coolant migration in these more complicated shaped channels with ribs and film cooling ejection holes. Entrance conditions are not smoothed and are similar to realistic channels resulting in strong entrance effects on channel heat transfer. The results from the current study were compared with correlation based predictions for the first pass rectangular channel for ribs and smooth surfaces. The correlation over-predicts the Nusselt number compared to the experimentally obtained Nusselt numbers. These results provide insight into using correlations developed for simplified geometries and idealistic flow conditions to predicting heat transfer for more realistic geometries. There is a need for more detailed studies on comparing predicted heat transfer results from correlations and actual measurements on realistic channels. With the current technique, it may also be easier to evaluate complete blade circuits for actual Nusselt numbers and operating conditions. These numbers can then be scaled up to engine conditions and used in design analysis.

NOMENCLATURE

D_h	channel hydraulic diameter (mm)
e	rib height (mm)
h	local heat transfer coefficient (W/m2-K)
L	length of channel (mm)
Nu_d	Nusselt number
Re_d	average channel Reynolds number
k	thermal conductivity of acrylic target surface(W/m-K)
k_{air}	thermal conductivity of air (W/m-K)
P	rib to rib spacing or pitch (mm)
t	time (seconds)
T_i	initial temperature of target surface (K)
T_w	wall surface temperature of target surface (K)
T_m	mainstream flow temperature (K)
V	average jet velocity (m/s)
x	streamwise distance along channel (mm)
α	thermal diffusivity of acrylic target surface (m^2/s)
ν	kinematic viscosity of fluid (m^2/s)

ACKNOWLEDGMENTS

The primary authors would like to acknowledge the support for the research from Rolls-Royce Corporation, Indianapolis.

REFERENCES

1. Han, J.C., 1984, "Heat transfer and Friction in Channels with Two Opposite Rib-Roughened Walls," ASME Journal of Heat Transfer, Vol. 106, Nov., pp. 774-781
2. Han, J.C., 1988, "Heat Transfer and Friction Characteristics in Rectangular Channels with Rib Turbulators," ASME Journal of Heat Transfer, Vol. 110, May, pp. 321-328.
3. Han, J.C., Zhang, Y.M., Lee, C.P., 1991, "Augmented Heat Transfer in Square Channels with Parallel, Crossed, and V-Shaped Ribs," ASME Journal of Heat Transfer, Vol.113, Oct., pp. 590-596.
4. Zhang, Y.M., Gu, W.Z., and Han, J.C., 1994, "Augmented Heat Transfer in Triangular Ducts with Full and Partial Ribbed Walls," AIAA Journal of Thermophysics and Heat Transfer, Vol. 8, July, pp. 574-579.
5. Taslim, M.,E., Li., T., and Spring, S.D., 1997, "Measurements of Heat Transfer Coefficients and Friction Factors in Rib-Roughened Channels Simulating Leading Edge Cavities of a Modern Turbine Blade," ASME Journal of Turbomachinery, Vol.119, Oct., pp. 601-609.
6. Ekkad, S.V., and Han, J.C., 1997, "Detailed Heat Transfer Distributions in Two-Pass Square Channels with Rib Turbulators," International Journal of Heat and Mass Transfer, Vol. 40, No.11, pp. 2525-2537.
7. Han, J.C., Dutta, S., and Ekkad, S.V., 2001, *Gas Turbine Heat Transfer and Cooling Technology*, Taylor & Francis, New York, New York.
8. Poser, R., Von Wolfersdorf, J., Lutum, E., Semmler, K., 2008, "Performing Heat Transfer Experiments in Blade Cooling Circuits Using a Transient Technique With Thermochromic Liquid Crystals," *ASME Turbo Expo 2008*, Berlin, June, GT2008-50364.
9. Esposito, E., Ekkad, S.V., Kim, Y.W., and Dutta, P., 2009, "Novel Jet Impingement Cooling Geometry for Combustor Liner Backside Cooling," ASME Journal of Thermal Science & Engineering Applications, June 2009, Vol. 1, 021001-1:8.
10. Ekkad, S.V., and Han, J.C., 2000, "A Transient Liquid Crystal Thermography Technique for Gas Turbine Heat Transfer Measurements," Measurement Science & Technology, Special Edition on Gas Turbine Measurements, July, Vol. 11, pp. 957-968.
11. Kline SJ, McClintock FA, 1953, "Describing uncertainties in single sample experiments," Mechanical Engineering, Vol. 75, pp. 3–8.
12. Ekkad, S.V., Huang, Y., and Han, J.C., 1998, "Detailed Heat Transfer Distributions in Two-Pass Square Channels with Rib Turbulators and Bleed Holes," International Journal of Heat and Mass Transfer, Vol. 41, pp. 3781-3791.